Suppressing Ion Migration Enables Stable Perovskite Light-Emitting Diodes with All-Inorganic Strategy

Lin Zhang, Fang Yuan,* Jun Xi, Bo Jiao, Hua Dong, Jingrui Li,* and Zhaoxin Wu*

Stability issue is one of the major concerns that limit emergent perovskite light-emitting diodes (PeLEDs) techniques. Generally, ion migration is considered as the most important origin of PeLEDs degradation. In this work, an all-inorganic device architecture, LiF/perovskite/LiF/ZnS/ZnSe, is proposed to address this imperative problem. The inorganic $(Cs_{1-x}Rb_x)_{1-y}K_yPbBr_3$ perovskite is optimized with achieving a photoluminescence quantum yield of 67%. Depth profile analysis of X-ray photoelectron spectroscopy indicates that the LiF/perovskite/LiF structure and the ZnS/ZnSe cascade electron transport layers significantly suppress the electric-field-induced ion migrations of the perovskite layers, and impede the diffusion of metallic atoms from cathode into perovskites. The as-prepared PeLEDs display excellent shelf stability (maintaining 90% of the initial external quantum efficiency [EQE] after 264 h) and operational stability (half-lifetime of about 255 h at an initial luminance of 120 cd m^{-2}). The devices also exhibit a maximum brightness of 15 6155 cd m^{-2} and an EQE of 11.05%.

1. Introduction

Perovskite light-emitting diodes (PeLEDs) have recently attracted tremendous attention. Various merits of lead halide perovskites, including the excellent photoluminescence quantum yield (PLQY), tunable band gap, high charge-carrier

L. Zhang, F. Yuan, Dr. B. Jiao, Dr. H. Dong, Prof. Z. Wu
Key Laboratory for Physical Electronics and Devices of the Ministry of Education & Shaanxi Key Lab of Information Photonic Technique
School of Electronic Science and Engineering
Xi'an Jiaotong University
Xi'an, Shaanxi 710049, P. R. China
E-mail: yuanf121@xjtu.edu.cn; zhaoxinwu@mail.xjtu.edu.cn
Dr. J. Xi
Zernike Institute for Advanced Materials
University of Groningen
Nijenborgh 4, Groningen AG 9747, The Netherlands
Prof. J. Li
Electronic Materials Research Laboratory
Key Laboratory of the Ministry of Education & International Center
for Dielectric Research
Faculty of Electronic and Information Engineering
Xi'an Jiaotong University
Xi'an, Shaanxi 710049, P. R. China
E-mail: jingrui.li@xjtu.edu.cn
Prof. Z. Wu
Collaborative Innovation Center of Extreme Optics
Shanxi University
Taiyuan, Shanxi 030006, P. R. China

mobility, and low cost, make this emergent technology very promising.[1–9] Recently, near-infrared and green PeLEDs with external quantum efficiency (EQE) over 20% were reported,[10–13] signifying that we are one step closer to the practical application of PeLEDs in lighting and displays.

Several metrics are generally used to assess the performance of PeLEDs. EQE and lifetime are of particular importance among them. Besides, brightness is an intuitive criterion for visible LEDs.[14–16] Most of the previous studies have not yet matched these three metrics simultaneously. For example, the green PeLED with the to-date record-high EQE of 20.3%, the record of PeLEDs so far, had a maximal luminance of 14 000 cd m^{-2} and 46 h lifetime (measured at continual mode of 100 cd m^{-2});[11] while for the most stable green PeLED to date (lifetime 250 h measured at initial brightness of 100 cd m^{-2}), the EQE and luminance were 10.5% and 16 436 cd m^{-2}, respectively.[17] Critical factors that affect the PeLEDs lifetime include the materials stability, the intrinsic defects in perovskites, and most importantly, ion migration within devices.[18–21] Stable perovskites with high luminescence are essential to achieve PeLEDs with both high stability and efficiency. Hybrid organic–inorganic perovskites degrade quickly against the heat and environmental moisture. All-inorganic perovskites usually have higher stability, but their PLQY is generally unsatisfactory because of the relatively low film quality.[22] The non-uniform morphology of perovskite films and the high density of defect states are detrimental to the electroluminescence (EL) emission. Intrinsic defects can mediate charge-carrier trapping thus leading to nonradiative recombination loss, which is harmful to the device performance. For efficient PeLEDs with high stability, many efforts have been devoted to reduce the trap states in perovskite films. Introducing large organic ligands is a widely adopted approach, as it can passivate defects and achieve a relatively high film quality by stabilizing the perovskite surfaces or facilitating the formation of low-dimensional perovskites.[13,23–27] Through optimal composition and phase engineering, Yang et al. achieved an EQE of 14.36% and an improved stability for green PeLEDs with quasi-2D perovskites.[27] Meanwhile, Xu et al. demonstrated a highly efficient and stable PeLEDs through the rational design of passivation molecules.[13] The improved stability results from a combination of reduced Joule heating caused by the high efficiency and the suppression of ion migration due to reduced defect density.

**ADVANCED
SCIENCE NEWS**
www.advancedsciencenews.com

**ADVANCED
FUNCTIONAL
MATERIALS**
www.afm-journal.de

Recently, Wang et al. improved the stability of the perovskite layer and demonstrated a stable PeLED with half-lifetime of 250 h at an initial luminance of 100 cd m^{-2}.[17] Nevertheless, the insulating nature of the organic ligands is disadvantageous to the charge transport and thus the device brightness.[28–30] In order to reduce the limitation of nonradiative losses and material instability on the device performance, the addition of alkali-metal ions into perovskites seems like a feasible pathway to decorate the surfaces and grain boundaries with passivating trap states.

Moreover, electric-field-induced ion migration has been demonstrated to significantly influence the operation lifetime of PeLEDs. There are two categories of ion migration in PeLEDs: ion exchange between the perovskite emission layer and charge-transport interlayers and ion penetration through them, and the diffusion of metallic atoms from the electrodes into and even through the charge-transport layers. They result in defect formation and materials degradation of both perovskite and interlayers, as well as electrode corrosion.[21,31,32] The deterioration of perovskite film during operation will lead to the rapid degradation of the EL performance. Several approaches have been proposed to improve device stability, such as addition of organic amine molecules or polymers,[17,23,33] nanostructured silica layers,[34,35] and introduction of metal-oxide layers.[36] Unfortunately, these methods have not yet demonstrated that they can realize relatively high brightness and efficiency of PeLED devices. Therefore, it is very important to improve the device architecture so that is can effectively suppress ion migrations and retain satisfactory device efficiency and brightness. Recently, an ultra-bright green PeLED (luminance 496 320 cd m^{-2}) was realized employing inorganic perovskite CsPbBr$_3$, inorganic Zn-Si-O electron-transport layer (ETL), and hybrid (organic–inorganic) hole-transport layer (HTL), with an EQE of 9.3%.[37]

In this work, we propose a simple and effective approach to highly stable green PeLEDs with an all-inorganic device architecture. Alkali-metal ions (Rb$^+$ and K$^+$) were added into the inorganic CsPbBr$_3$ perovskite to passivate trap states and optimize the film quality. Importantly, to suppress electric-field-induced ion migrations, a pair of ultrathin LiF layers were used to sandwich the perovskite emission layer, forming an "insulator–perovskite–insulator" (IPI) device structure,[38–40] and a combination of inorganic ZnS/ZnSe were used as cascade ETLs. The impact of these strategies was demonstrated by depth profile analysis of X-ray photoelectron spectroscopy (D-XPS). The IPI strategy which we developed earlier can effectively hinder ion migration between perovskite and charge-transport layers, suppress interfacial exciton quenching, and induce charge injection via tunneling effect.[38] As an alternative to the traditional organic ETLs, the compact inorganic ETLs can successfully inhibit the diffusion of cathodic metal atoms toward the perovskite layer. Therewith ion migrations via both channels were minimized. Inorganic ETLs can largely mitigate the device degradation caused by the Joule-heating effect, which is detrimental to organic charge-transport materials due to their low glass-transition temperatures.[41,42] In addition, the cascade ZnS/ZnSe ETLs can reduce energy barriers and increase charge-injection rates. With this all-inorganic LiF/(Cs/Rb/K) PbBr$_3$/LiF/ZnS/ZnSe architecture, we achieved all-inorganic green PeLEDs retaining a bright emission (156 155 cd m^{-2}),

a maximum current efficiency of 35.15 cd A^{-1}, and a peak EQE of 11.05%. Most importantly, our devices exhibit an excellent shelf lifetime as 90% of the initial EQE was maintained after 264 h, and operational lifetime of about 255 h (measured at the initial luminance of 120 cd m^{-2}). We anticipate that the all-inorganic strategy proposed here could be a common method for improving the device performance of PeLEDs.

2. Results and Discussion

Figure 1a illustrates a facile preparation procedure of all-inorganic perovskite films by a chlorobenzene-assisted pre-annealing process (CPA) treatment (see the Experimental Section for details). The scanning electron microscopy (SEM) images, X-ray diffraction (XRD) patterns, and PL spectra evolution of CPA treated and untreated films are summarized in Figures S1–S4, Supporting Information. It can be seen that a proper CPA treatment time has a positive impact on the perovskite film formation. To further optimize the film quality, we introduced a small amount of alkali-metal cations into the perovskites. Compared to pure Cs films (Figure 1b), the bication (Cs$_{1-x}$Rb$_x$)PbBr$_3$ composition (denoted as Cs$_{1-x}$Rb$_x$, with $x = 0$, 0.06, 0.11, 0.17, 0.22, and 0.28) films exhibit increased surface coverage and reduced crystal grains, of which Cs$_{0.83}$Rb$_{0.17}$ (Figure 1c) shows the strongest effects (Figure S5, Supporting Information). With further addition of K$^+$ into the Cs$_{0.83}$Rb$_{0.17}$ precursor solution, the trication ((Cs$_{0.83}$Rb$_{0.17}$)$_{1-y}$K$_y$)PbBr$_3$ (abbreviated as (Cs$_{0.83}$Rb$_{0.17}$)$_{1-y}$K$_y$ hereafter) films were fabricated. As reported elsewhere, this composition might contain a slight excess of halide that could compensate halide vacancies.[8] In our case, the trication approach results in uniform and pinhole-free surface morphology with homogeneous crystal domains (Figure 1d and Figure S6, Supporting Information). Atomic force microscopy (AFM) characterization (Figure S7, Supporting Information) shows the significantly reduced surface roughness of the trication perovskite films with smaller and denser grains. Agreeing with the film-quality trends, the Cs$_{0.83}$Rb$_{0.17}$ and (Cs$_{0.83}$Rb$_{0.17}$)$_{0.95}$K$_{0.05}$ films exhibit the highest PL intensity among the bication and trication perovskites, respectively (Figure S8, Supporting Information). As shown in Figure 1e, the PLQY increases to 67% for the (Cs$_{0.83}$Rb$_{0.17}$)$_{0.95}$K$_{0.05}$ film, with the intensity of excitonic absorption peak becoming obviously larger (Figure S9, Supporting Information).

The time-resolved PL spectra show that the (Cs$_{0.83}$Rb$_{0.17}$)$_{0.95}$K$_{0.05}$ film has a 2.6-fold average lifetime than that of pure Cs film (Figure 1f and Table S1, Supporting Information), revealing significantly decreased defect density owing to the trication approach. The passivation effects on trap states can be estimated by pump-fluence-dependent PL measurements (Figure 1g). It can be seen that in the trication sample, the threshold point of emission intensity is reduced, corresponding to decreased defect density. The corresponding XRD patterns, energy dispersive spectroscopy, and X-ray photoelectron spectroscopy (XPS) data (Figures S10–S12, Supporting Information) further confirm the crystallinity, composition, and chemical states of these perovskite films. Moreover, the PL mappings have clarified the positive effect of additives incorporation on the emission intensity of perovskite films (Figure S13, Supporting Information).
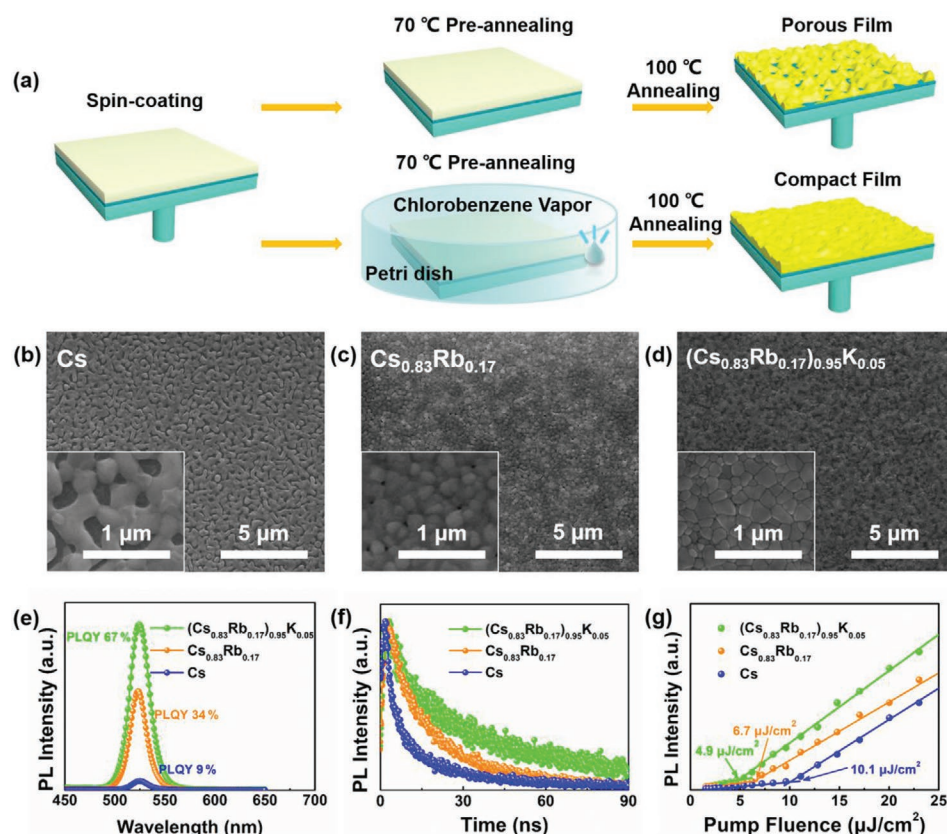
Figure 1. a) Schematic illustration of the formation process for the perovskite films. The perovskite precursor solution was one-step spin coated on the glass/LiF substrate, followed by the chlorobenzene-assisted pre-annealing process (CPA) treatment immediately, and then annealed at high temperature to form perovskite films. SEM images of b) Cs, c) $Cs_{0.83}Rb_{0.17}$, and d) $(Cs_{0.83}Rb_{0.17})_{0.95}K_{0.05}$ perovskite films. e) Steady-state PL spectra and PLQYs of the Cs, $Cs_{0.83}Rb_{0.17}$ and $(Cs_{0.83}Rb_{0.17})_{0.95}K_{0.05}$ films. f) Time-resolved PL spectra of these perovskite films. g) PL intensity of perovskite films as a function of pump intensity. The inflection point of the fitted curves indicates that the traps are filled, meanwhile the corresponding pump intensity is the pump fluence threshold (P_{th}) of traps. The P_{th} of the Cs ($Cs_{0.83}Rb_{0.17}$) film is 10.1 (6.7) µJ cm^{-2}, corresponding to a trap state density of about 7.25×10^{17} (4.81×10^{17}) cm^{-3}. For the $(Cs_{0.83}Rb_{0.17})_{0.95}K_{0.05}$ film, the trap state density decreases to 3.52×10^{17} cm^{-3} (4.9 µJ cm^{-2}), which is consistent with the decreased nonradiative losses.

Based on the organic-moiety-free perovskite films with optimized composition, we fabricated the novel all-inorganic IPI-structured PeLEDs which were composed of the device architecture (**Figure 2**a) ITO/LiF (3 nm)/perovskite (≈70 nm)/LiF (7 nm)/ZnS (30-d nm)/ZnSe (d nm)/Ag (100 nm). Apart from the solution processed perovskite emitting layer, all other layers were deposited in vacuum chamber. Notably, the first LiF layer was unavailable to be dissolved by perovskite precursor solutions. The corresponding band alignment of all functional layers obtained from the ultraviolet photoelectron spectroscopy (UPS) spectra (Figure 2b,c and Figure S14, Supporting Information) was given. The optimization of LiF interlayers and the mechanism of the IPI-structured PeLEDs can be found in our previous works.[38–40] The first LiF layer replaces the conventional HTL to improve the hole injection into perovskite emitting layer via tunneling effect. The second LiF layer bridges the perovskite emitting layer and ETLs, as well as prevents the luminescence quenching at the interface (Figure S15, Supporting Information). The ZnS and ZnSe were used as ETLs and holes blocking layers.[45,46] The Hall measurement of evaporated ZnS and ZnSe films is shown in Table S2, Supporting Information. Besides, the combination of ZnS and ZnSe layer

(overall thickness 30 nm) can act as cascade ETLs to reduce energy barriers for high efficient electron injections from the metal cathode to perovskite.

To further confirm the optimization of perovskite films, we characterized the device performance with varying the emission-layer composition and fixing the ZnSe thickness to 3 nm (i.e., d is 3). The current luminance–voltage–density (L–V–J), CE–voltage (CE–V), and the corresponding EQE–voltage (EQE–V) characteristics of PeLEDs based on Cs, $Cs_{0.83}Rb_{0.17}$, and $(Cs_{0.83}Rb_{0.17})_{0.95}K_{0.05}$ perovskite films are summarized in Figure S16, Supporting Information. It is found from the J–V curves that the Cs-based device exhibits a higher injection current at low voltage, which is not surprising in view of its poor surface coverage that induces current leakage. The maximum luminance (56 198 cd m^{-2}) of the $Cs_{0.83}Rb_{0.17}$-based PeLEDs is much higher than that of the Cs-based ones (27 980 cd m^{-2}). In addition, the maximum CE (17.31 cd A^{-1}) and EQE (5.26%) of the $Cs_{0.83}Rb_{0.17}$-based PeLEDs are also higher than that of Cs-based ones (8.63 cd A^{-1} and 2.28%). For the PeLED based on trication $(Cs_{0.83}Rb_{0.17})_{0.95}K_{0.05}$ film, the maximum luminance dramatically increases to 97 881 cd m^{-2}, along with the maximum CE to 25.97 cd A^{-1} and EQE to 8.16%. We analyzed the
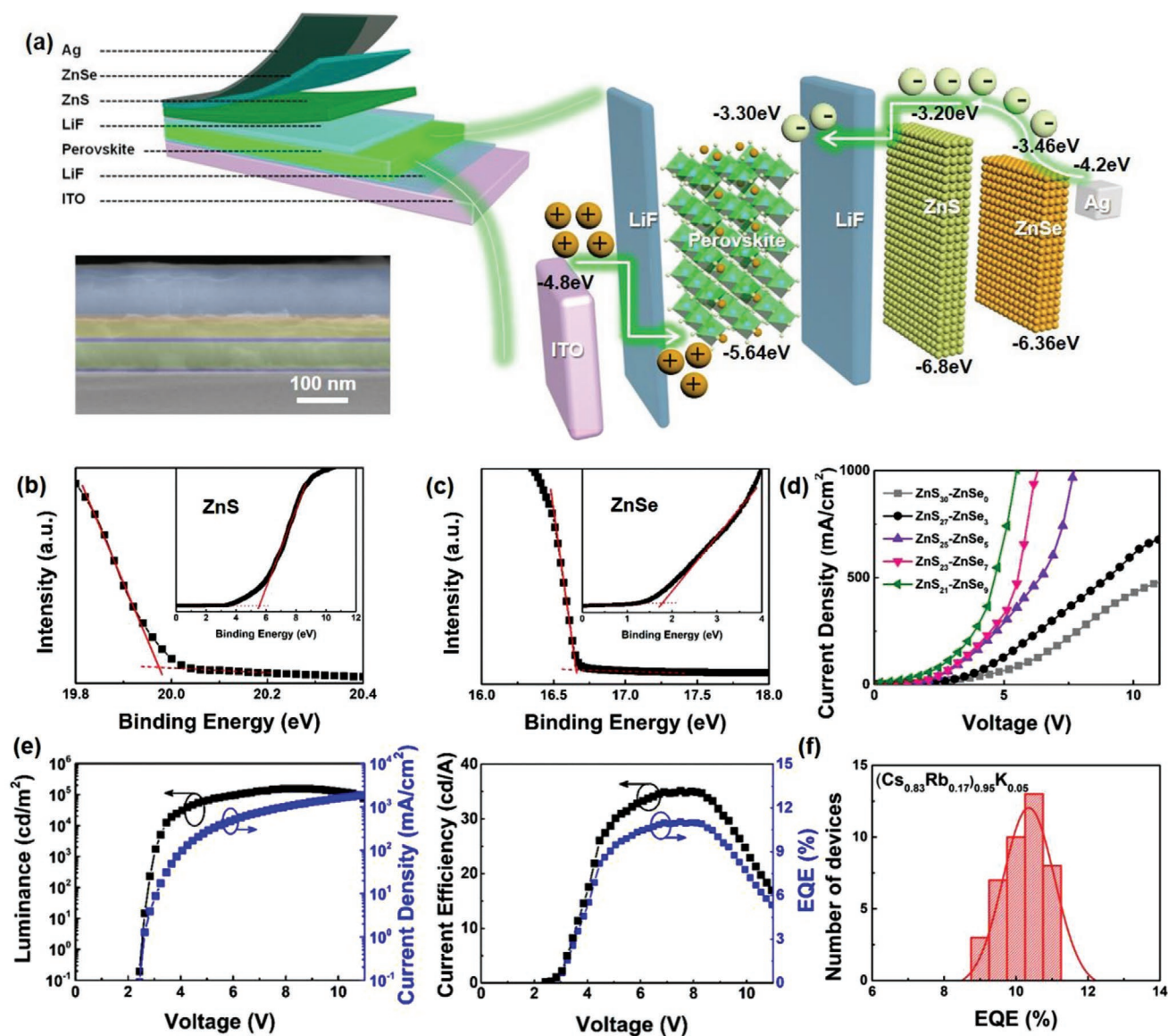
Figure 2. EL performance of the devices. a) Device structure and cross-sectional SEM image of all-inorganic PeLED. UPS spectra of b) ZnS and c) ZnSe layer. The WF of ZnS and ZnSe are −1.25 eV and −4.56 eV, respectively. The VBM can be estimated by −1.25 eV − 5.55 eV = −6.8 eV for ZnS and −4.56 eV − 1.8 eV = −6.36 eV for ZnSe, respectively. The CBM for ZnS and ZnSe layer are −3.2 and −3.46 eV, while their band gap values are extracted from the literature.[43,44] d) The current density–voltage characteristic of electron-only devices. The device architecture is ITO/zinc oxide (40 nm)/perovskite (around 70 nm)/ZnS-ZnSe ETLs (30 nm)/Ag (100 nm). e) Luminance–voltage (*L–V*) and current density–voltage (*J–V*), current efficiency-voltage (CE–V), and EQE–voltage (EQE–V) curves of $(Cs_{0.83}Rb_{0.17})_{0.95}K_{0.05}$-based PeLED with ZnS (23 nm)/ZnSe (7 nm) ETLs. f) Histograms of EQE for $(Cs_{0.83}Rb_{0.17})_{0.95}K_{0.05}$-based PeLEDs with ZnS (23 nm)/ZnSe (7 nm) ETLs and obtained from over 40 individual devices.

current distribution on the surfaces of these perovskite films using conductive AFM measurement (Figure S17, Supporting Information). As discussed above, the introduction of alkali additives into $CsPbBr_3$ led to uniform, pinhole-free, and dense perovskite film with higher PLQY. Low and uniformly distributed current density in $(Cs_{0.83}Rb_{0.17})_{0.95}K_{0.05}$ film is expected due to the minimized leakage current that leads to increased capture rate of electron–hole carriers.

It can be foreseen that the conductivity of ZnSe in the cascade ETLs could lower the charge-injection barrier and facilitate charge injection into the emitting layer, so as to enhance the device efficiency and brightness. In this regard, we further

optimized the thickness combination of ZnS-ZnSe ETLs in $(Cs_{0.83}Rb_{0.17})_{0.95}K_{0.05}$-based PeLEDs (Figure S18 and Table S3, Supporting Information). It can be found that the control device ($d = 0$, i.e., ZnS only) is associated with the lowest EL efficiency and luminance, which results from large electron-injection barrier between ZnS and Ag electrode. With increasing thickness of the ZnSe, the light turn-on voltage (V_{on}, defined for the luminance of 1 cd m^{-2}) significantly decreases. To investigate the effect of cascade ZnS-ZnSe ETLs on the charge-injection efficiency, the electron-only devices have been fabricated (Figure 2d). As the thickness of ZnSe increases, devices with cascade ZnS-ZnSe ETLs show increasing current density as
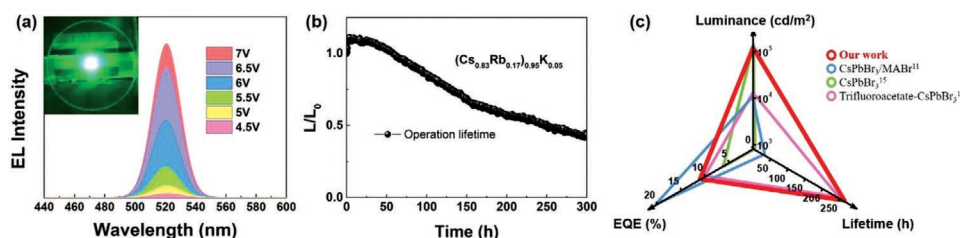
Figure 3. a) EL spectra of the PeLED at various biases (the emission image is shown in the inset). b) Operational lifetime (T_{50}) of the $(Cs_{0.83}Rb_{0.17})_{0.95}K_{0.05}$-based device with L_0 of 120 cd m^{-2}. c) The EL performance of our and previous reported devices.[11,15,17]

expected.[47,48] By carefully optimizing the thickness of the ZnSe layer, the ZnS (23 nm)/ZnSe (7 nm) PeLED achieved the best performance with peak CE and EQE of 35.15 cd A^{-1} and 11.05% at ≈545 mA cm^{-2} (around 143 700 cd m^{-2}). The maximum luminance of device is 156 155 cd m^{-2}, much higher than that of other combinations. Furthermore, these $(Cs_{0.83}Rb_{0.17})_{0.95}K_{0.05}$-based PeLEDs with ZnS (23 nm)/ZnSe (7 nm) ETLs also demonstrated good reproducibility (Figure 2f).

We highlight that our IPI-structured PeLEDs exhibit excellent stability. As shown in **Figure 3**a, the EL spectra of $(Cs_{0.83}Rb_{0.17})_{0.95}K_{0.05}$-based device exhibits no obvious peak drift as the voltage bias increases from 4.5 to 7 V. Meanwhile, the shelf stability of unencapsulated $(Cs_{0.83}Rb_{0.17})_{0.95}K_{0.05}$-based PeLED stored in N$_2$ glovebox (i.e., the device efficiency was measured at intervals of 24 h) is shown in Figure S19, Supporting Information. After 264 h, 90% of the initial EQE value was maintained. The high shelf stability of $(Cs_{0.83}Rb_{0.17})_{0.95}K_{0.05}$-based PeLEDs can be attributed to the dense, smooth, and pinhole-free perovskite films. High shelf stability is the base of long-term stability of PeLEDs, which is critical for lighting and displaying applications. Here we take the concept of half-lifetime (T_{50}) to evaluate the device operational stability, which is defined as the time required for the luminance of device to decease to 50% of its initial luminance (L_0). The measured T_{50} of the $(Cs_{0.83}Rb_{0.17})_{0.95}K_{0.05}$-based PeLED is about 255 h

(Figure 3b), much longer than that of Cs-based (95 h) and $Cs_{0.83}Rb_{0.17}$-based (139 h) ones (Figure S20, Supporting Information). Compared with some representative green PeLEDs listed in **Table 1** and Figure 3c,[11,14,15,17,27,37,49–54] we can claim that our all-inorganic strategy has realized the improved operational stability with retaining high brightness and reasonably high efficiency. For practical application of all-inorganic PeLEDs in the high brightness region, we also checked the operational stability of $(Cs_{0.83}Rb_{0.17})_{0.95}K_{0.05}$-based PeLED at around 1000 cd m^{-2} (Figure S21, Supporting Information).

Such superior performance (particular operational stability) of our PeLEDs is attributed to both materials and device architecture. In regard to materials, all-inorganic perovskites have higher thermal stability than the hybrid (methylammonium- and formamidinium-based) analogues.[55,56] The alkali-metal additives can effectively passivate defects without inducing loss in charge-carrier mobility,[57] thus leading to remarkable improvement of device brightness. PL measurements of perovskite films before and after operation (Figure S22, Supporting Information) indicate that the introduction of Rb$^+$ and K$^+$ ions also improved the thermal stability of perovskite film. Moreover, the device architecture without using traditional organic charge-transport layers, such as poly(3,4-ethylenedioxythiophene) polystyrene sulfonate (PEDOT:PSS) as HTL and 2,2′,2″-(1,3,5-benzenetriyl)-tris(1-phenyl-1-H-benzimidazole

Table 1. Performance summary of the representative PeLEDs.

Emitter	EL peak [nm]	V_{on} [V]	L_{max} [cd m^{-2}]	EQE_{max} [%]	CE_{max} [cd A^{-1}]	Lifetime	Reference
$(Cs_{0.83}Rb_{0.17})_{0.95}K_{0.05}PbBr_3$	519	2.4	156 155	11.05	35.15	255 h (L_0: 120 cd m^{-2})	Our work
$CsPbBr_3$/MABr	525	2.7	14 000	20.3	78	46 h (L: 100 cd m^{-2})*	[11]
$Cs_{0.87}MA_{0.13}PbBr_3$	520	2.9	91 000	10.43	33.9	40 s (L_0: 610 cd m^{-2})	[14]
$CsPbBr_3$	522	2.43	179 000	7.39	28.00	6 h (L_0: 100 cd m^{-2})	[15]
Trifluoroacetate-$CsPbBr_3$	518	2.8	16 436	10.5	32.0	250 h (L_0: 100 cd m^{-2})	[17]
$PEA_2(FAPbBr_3)_{n-1}PbBr_4$	532	–	9120	14.36	62.4	65 min (L_0: 270 cd m^{-2})	[27]
$CsPbBr_3$	523	2.5	496 320	9.3	37	60 min (L_0: 5500 cd m^{-2})	[37]
$(OA)_2(FA)_{n-1}Pb_nBr_{3n+1}$	528	2.2	56 143	13.4	57.6	800 s (L_0: 105 cd m^{-2})	[49]
$MAPbBr_3$	–	3.1	22 830	12.9	–	6 min (L_0: 100 cd m^{-2})	[50]
$CsPbBr_3$	524	2.8	7267	0.15	0.57	>15 h (L> 100 cd m^{-2})*	[51]
$CsPbBr_3$	527	–	10 700	0.93	2.90	1.3 h (L_0: 470 cd m^{-2})	[52]
$MAPbBr_3$	–	2.8	55 400	12.1	55.2	135 min#	[53]
$CsPbBr_3$	522	–	13 752	1.37	5.39	<1.25 h (L_0: 100 cd m^{-2})	[54]

V_{on}, turn-on voltage; L_{max}, EQE_{max}, and CE_{max}, the maximal luminance, EQE, and current efficiency.
Labels for the lifetime data—unlabeled, T_{50} measured at initial luminance L_0; *, lifetime measured in continual model at L; #. T_{50} with L_0 unindicated.

**ADVANCED
SCIENCE NEWS**

www.advancedsciencenews.com

**ADVANCED
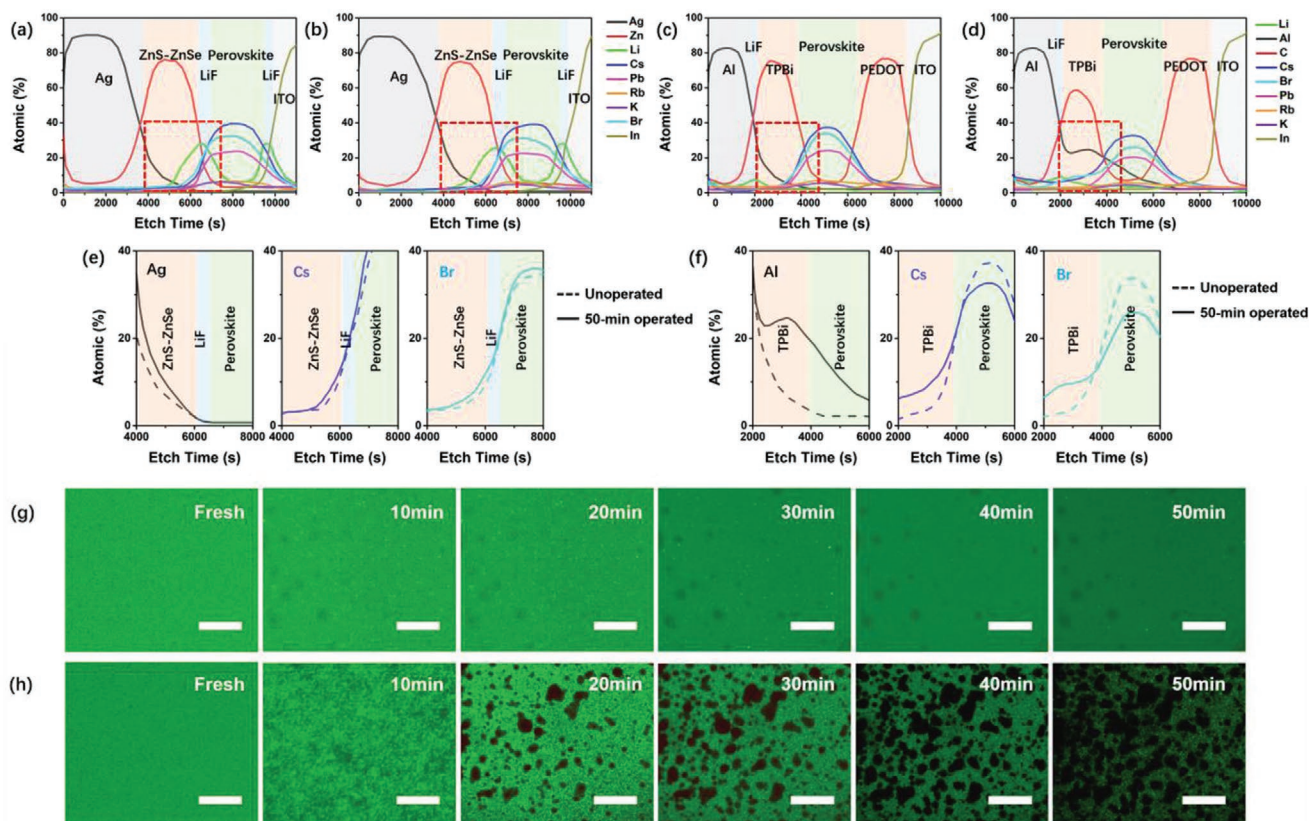FUNCTIONAL
MATERIALS**

www.afm-journal.de

Figure 4. Operational stability characteristics of the PeLEDs. The initial luminance of device was 1000 cd m^{-2}. The depth profile analysis of X-ray photo-electron spectroscopy (D-XPS) for a) unoperated and b) 50 min operated IPI device, respectively. The D-XPS measurement of c) unoperated and d) 50 min operated control device, respectively. e) Element distribution of Ag, Cs, and Br for unoperated and 50 min operated IPI device. f) Element distribution of Al, Cs, and Br for unoperated and 50 min operated control device. The real-time luminance degradation images of g) IPI and h) control device. Scale bar is 20 μm.

(TPBi) as ETL, avoids the concerns of the instability of these materials against heat and high current density. With respect to device structure, efficiencies of both charge-carrier transport and injection were improved upon the use of the IPI structure and the optimized cascade ZnS-ZnSe ETLs.

Especially, the IPI structure and cascade ZnS-ZnSe ETLs in our all-inorganic strategy significantly suppressed the ion migration, which is regarded as the decisive factor for operational instability of PeLEDs. We carried out D-XPS measurements to explore the electric-field-induced ion migration in devices. The relative percentage change of in-depth distribution of the elements as a function of the etching time for unoperated and 50 min operated devices (the L_0 is around 1000 cd m^{-2}) was investigated by two typical device architectures: the IPI-structured, ZnS-ZnSe-containing device, and the conventional device as a control one (ITO/PEDOT:PSS (40 nm)/$(Cs_{0.83}Rb_{0.17})_{0.95}K_{0.05}$ perovskites (≈70 nm)/TPBi (30 nm)/LiF (1 nm)/Al (100 nm)). The D-XPS images of corresponding devices are shown in **Figure 4**a–f with the XPS measurements given in Figure S23, Supporting Information. Each layer of PeLEDs has its representative element: Al or Ag for the metal electrodes; Li for LiF layer; C for both PEDOT:PSS and TPBi; Zn for ZnS-ZnSe; Cs, Pb, Br, Rb, and K for the perovskite; and In for ITO. Very different results were observed with

these two devices. For the all-inorganic PeLED, there is negligible difference between the D-XPS profiles of unoperated and operated devices. All investigated elements remained still confined in their corresponding layers after 50 min operation time. This indicates that ion migration processes at interfaces were substantially inhibited due to the huge barriers induced by the compact inorganic interlayer and insulating layers on both sides. There was even no ion accumulation observed at the interface. In contrast, for the control device, significant Al diffusion through the TPBi layer into the perovskite was clearly seen, so was the Cs and Br diffusion in the opposite direction. Besides, Figure S23, Supporting Information shows a peak at around 74.50 eV for Al 2p, indication the formation of Al$_2$O$_3$ during operation. Overall, D-XPS results reveal that the all-inorganic IPI device architecture successfully suppressed the ion migration, which was more stable than the control device with traditional device with organic components. These results are consistent with the magnified operation images of PeLED during operation under constant applied current (the L_0 is around 1000 cd m^{-2}) (Figure 4g,h). It can be seen that the large emission areas in control device gradually darkened with increasing operation time. The generation of these black spots is most likely caused by the severe ion migrations. The negligible luminance degradation of all-inorganic device would be

ADVANCED
SCIENCE NEWS
www.advancedsciencenews.com

ADVANCED
FUNCTIONAL
MATERIALS
www.afm-journal.de

a direct evidence of IPI architecture on the operational stability. These findings could provide an effective guidance for better understanding and improvement of device stability.

In general, pure halide perovskites can prevent halide phase segregation caused by ion migration within the perovskite layer, and also efficiently avoid halide ions piled up at the interfaces which results in larger injection barriers.[58] For the conventional organic light-emitting diodes, the influence of metal diffusion from electrodes into the light-emitting layer on the device reliability has already been discussed.[59–61] Huang et al. revealed Al penetration into the emission layer and pointed out its strong correlation with the luminescence quenching.[59] It was reported that metal diffusion from the anode can be inhibited through the insertion of insulating layers.[61] We believe that these concepts can be adopted for PeLEDs. That is, the inhibition of metal migration and ion migration of perovskite is crucial for the device operational stability, and the inorganic layer acts as a protection barrier to effectively suppress the interfacial ions migration processes. Therewith the stability of perovskite film and other functional layers is guaranteed.

3. Conclusion

In summary, we demonstrate the high-performance PeLEDs through the rational design of all-inorganic strategy that can synergistically integrate inorganic device architecture and high-quality inorganic perovskite films. The organic-moieties-free design of perovskite greatly enhanced the radiative efficiency and film stability through defect passivation and composition modulation. What is the most distinguished is a practical design of IPI device structure coupled with a cascade ZnS-ZnSe ETLs. This novel structure not only significantly avoids the device degradation caused by either ion migration or heat, but also allows high charge-injection efficiency into perovskites. This strategy could open an avenue for the PeLED community, and provides valuable insights into the device stability.

Supporting Information

Supporting Information is available from the Wiley Online Library or from the author.

Conflict of Interest

The authors declare no conflict of interest.

[1] A. Mei, X. Li, L. Liu, Z. Ku, T. Liu, Y. Rong, M. Xu, M. Hu, J. Chen, Y. Yang, M. Grätzel, H. Han, *Science* **2014**, *345*, 295.

[2] H. Cho, S. H. Jeong, M. H. Park, Y. H. Kim, C. Wolf, C. L. Lee, J. H. Heo, A. Sadhanala, N. Myoung, S. Yoo, S. H. Im, R. H. Friend, T. W. Lee, *Science* **2015**, *350*, 1222.

[3] G. E. Eperon, T. Leijtens, K. A. Bush, R. Prasanna, T. Green, J. T.-W. Wang, D. P. McMeekin, G. Volonakis, R. L. Milot, R. May, A. Palmstrom, D. J. Slotcavage, R. A. Belisle, J. B. Patel, E. S. Parrott, R. J. Sutton, W. Ma, F. Moghadam, B. Conings, A. Babayigit, H.-G. Boyen, S. Bent, F. Giustino, L. M. Herz, M. B. Johnston, M. D. McGehee, H. J. Snaith, *Science* **2016**, *354*, 861.

[4] J. Xi, Z. Wu, B. Jiao, H. Dong, C. Ran, C. Piao, T. Lei, T.-B. Song, W. Ke, T. Yokoyama, X. Hou, M. G. Kanatzidis, *Adv. Mater.* **2017**, *29*, 1606964.

[5] J. Xi, C. Piao, J. Byeon, J. Yoon, Z. Wu, M. Choi, *Adv. Mater.* **2019**, *9*, 1901787.

[6] L. Zhang, F. Yuan, H. Dong, B. Jiao, W. Zhang, X. Hou, S. Wang, Q. Gong, Z. Wu, *ACS Appl. Mater. Interfaces* **2018**, *10*, 40661.

[7] Y. Jiang, C. Qin, M. Cui, T. He, K. Liu, Y. Huang, M. Luo, L. Zhang, H. Xu, S. Li, J. Wei, Z. Liu, H. Wang, G.-H. Kim, M. Yuan, J. Chen, *Nat. Commun.* **2019**, *10*, 1868.

[8] M. Abdi-Jalebi, Z. Andaji-Garmaroudi, S. Cacovich, C. Stavrakas, B. Philippe, J. M. Richter, M. Alsari, E. P. Booker, E. M. Hutter, A. J. Pearson, S. Lilliu, T. J. Savenije, H. Rensmo, G. Divitini, C. Ducati, R. H. Friend, S. D. Stranks, *Nature* **2018**, *555*, 497.

[9] Y. Miao, Y. Ke, N. Wang, W. Zou, M. Xu, Y. Cao, Y. Sun, R. Yang, Y. Wang, Y. Tong, W. Xu, L. Zhang, R. Li, J. Li, H. He, Y. Jin, F. Gao, W. Huang, J. Wang, *Nat. Commun.* **2019**, *10*, 3624.

[10] Y. Cao, N. Wang, H. Tian, J. Guo, Y. Wei, H. Chen, Y. Miao, W. Zou, K. Pan, Y. He, H. Cao, Y. Ke, M. Xu, Y. Wang, M. Yang, K. Du, Z. Fu, D. Kong, D. Dai, Y. Jin, G. Li, H. Li, Q. Peng, J. Wang, W. Huang, *Nature* **2018**, *562*, 249.

[11] K. Lin, J. Xing, L. N. Quan, F. P. G. de Arquer, X. Gong, J. Lu, L. Xie, W. Zhao, D. Zhang, C. Yan, W. Li, X. Liu, Y. Lu, J. Kirman, E. H. Sargent, Q. Xiong, Z. Wei, *Nature* **2018**, *562*, 245.

[12] B. Zhao, S. Bai, V. Kim, R. Lamboll, R. Shivanna, F. Auras, J. M. Richter, L. Yang, L. Dai, M. Alsari, X.-J. She, L. Liang, J. Zhang, S. Lilliu, P. Gao, H. J. Snaith, J. Wang, N. C. Greenham, R. H. Friend, D. Di, *Nat. Photonics* **2018**, *12*, 783.

[13] W. Xu, Q. Hu, S. Bai, C. Bao, Y. Miao, Z. Yuan, T. Borzda, A. J. Barker, E. Tyukalova, Z. Hu, M. Kawecki, H. Wang, Z. Yan, X. Liu, X. Shi, K. Uvdal, M. Fahlman, W. Zhang, M. Duchamp, J.-M. Liu, A. Petrozza, J. Wang, L.-M. Liu, W. Huang, F. Gao, *Nat. Photonics* **2019**, *13*, 418.

[14] L. Zhang, X. Yang, Q. Jiang, P. Wang, Z. Yin, X. Zhang, H. Tan, Y. M. Yang, M. Wei, B. R. Sutherland, E. H. Sargent, J. You, *Nat. Commun.* **2017**, *8*, 15640.

[15] X. Liu, X. Guo, Y. Lv, Y. Hu, Y. Fan, J. Lin, X. Liu, X. Liu, *Adv. Opt. Mater.* **2018**, *6*, 1801245.

[16] L. Song, X. Guo, Y. Hu, Y. Lv, J. Lin, Y. Fan, N. Zhang, X. Liu, *Nanoscale* **2018**, *10*, 18315.

[17] H. Wang, X. Zhang, Q. Wu, F. Cao, D. Yang, Y. Shang, Z. Ning, W. Zhang, W. Zheng, Y. Yan, S. V. Kershaw, L. Zhang, A. L. Rogach, X. Yang, *Nat. Commun.* **2019**, *10*, 665.

[18] L. Zhao, J. Gao, Y. L. Lin, Y.-W. Yeh, K. M. Lee, N. Yao, Y.-L. Loo, B. P. Rand, *Adv. Mater.* **2017**, *29*, 1605317.

[19] Z. Wei, J. Xing, *J. Phys. Chem. Lett.* **2019**, *10*, 3035.

[20] S. A. Veldhuis, P. P. Boix, N. Yantara, M. Li, T. C. Sum, N. Mathews, S. G. Mhaisalkar, *Adv. Mater.* **2016**, *28*, 6804.

[21] H. Cho, Y.-H. Kim, C. Wolf, H.-D. Lee, T.-W. Lee, *Adv. Mater.* **2018**, *30*, 1704587.

[22] Y. Ling, Y. Tian, X. Wang, J. C. Wang, J. M. Knox, F. Perez-Orive, Y. Du, L. Tan, K. Hanson, B. Ma, H. Gao, *Adv. Mater.* **2016**, *28*, 8983.

[23] Z. Xiao, R. A. Kerner, L. Zhao, N. L. Tran, K. M. Lee, T.-W. Koh, G. D. Scholes, B. P. Rand, *Nat. Photonics* **2017**, *11*, 108.

[24] L.-P. Cheng, J.-S. Huang, Y. Shen, G.-P. Li, X.-K. Liu, W. Li, Y.-H. Wang, Y.-Q. Li, Y. Jiang, F. Gao, C.-S. Lee, J.-X. Tang, *Adv. Opt. Mater.* **2019**, *7*, 1801534.

[25] N. Wang, L. Cheng, R. Ge, S. Zhang, Y. Miao, W. Zou, C. Yi, Y. Sun, Y. Cao, R. Yang, Y. Wei, Q. Guo, Y. Ke, M. Yu, Y. Jin, Y. Liu, Q. Ding, D. Di, L. Yang, G. Xing, H. Tian, C. Jin, F. Gao, R. H. Friend, J. Wang, W. Huang, *Nat. Photonics* **2016**, *10*, 699.

[26] M. Yuan, L. N. Quan, R. Comin, G. Walters, R. Sabatini, O. Voznyy, S. Hoogland, Y. Zhao, E. M. Beauregard, P. Kanjanaboos, Z. Lu, D. H. Kim, E. H. Sargent, *Nat. Nanotechnol.* **2016**, *11*, 872.

[27] X. Yang, X. Zhang, J. Deng, Z. Chu, Q. Jiang, J. Meng, P. Wang, L. Zhang, Z. Yin, J. You, *Nat. Commun.* **2018**, *9*, 570.

[28] H.-D. Lee, H. Kim, H. Cho, W. Cha, Y. Hong, Y.-H. Kim, A. Sadhanala, V. Venugopalan, J. S. Kim, J. W. Choi, C.-L. Lee, D. Kim, H. Yang, R. H. Friend, T.-W. Lee, *Adv. Funct. Mater.* **2019**, *29*, 1901225.

[29] M. Yu, C. Yi, N. Wang, L. Zhang, R. Zou, Y. Tong, H. Chen, Y. Cao, Y. He, Y. Wang, M. Xu, Y. Liu, Y. Jin, W. Huang, J. Wang, *Adv. Opt. Mater.* **2019**, *7*, 1801575.

[30] X. Zhang, C. Wang, Y. Zhang, X. Zhang, S. Wang, M. Lu, H. Cui, S. V. Kershaw, W. W. Yu, A. L. Rogach, *ACS Energy Lett.* **2019**, *4*, 242.

[31] H. Lee, D. Ko, C. Lee, *ACS Appl. Mater. Interfaces* **2019**, *11*, 11667.

[32] S. Lee, J. H. Park, B. R. Lee, E. D. Jung, J. C. Yu, D. D. Nuzzo, R. H. Friend, M. H. Song, *J. Phys. Chem. Lett.* **2017**, *8*, 1784.

[33] C. Wu, Y. Zou, T. Wu, M. Ban, V. Pecunia, Y. Han, Q. Liu, T. Song, S. Duhm, B. Sun, *Adv. Funct. Mater.* **2017**, *27*, 1700338.

[34] S. Park, J. Cho, D. Jeong, J. Jo, M. Nam, H. Rhee, J. S. Han, Y. J. Cho, B.-K. Ju, D.-H. Ko, H. S. Jang, *Chem. Eng. J.* **2020**, *393*, 124767.

[35] P. Cao, B. Yang, F. Zheng, L. Wang, J. Zou, *Ceram. Int.* **2020**, *46*, 3882.

[36] Z. Shi, Y. Li, Y. Zhang, Y. Chen, X. Li, D. Wu, T. Xu, C. Shan, G. Du, *Nano Lett.* **2017**, *17*, 313.

[37] K. Sim, T. Jun, J. Bang, H. Kamioka, J. Kim, H. Hiramatsu, H. Hosono, *Appl. Phys. Rev.* **2019**, *6*, 031402.

[38] Y. Shi, W. Wu, H. Dong, G. Li, K. Xi, G. Divitini, C. Ran, F. Yuan, M. Zhang, B. Jiao, X. Hou, Z. Wu, *Adv. Mater.* **2018**, *30*, 1800251.

[39] F. Yuan, J. Xi, H. Dong, K. Xi, W. Zhang, C. Ran, B. Jiao, X. Hou, A. K. Y. Jen, Z. Wu, *Phys. Status Solidi RRL* **2018**, *12*, 1800090.

[40] F. Yuan, C. Ran, L. Zhang, H. Dong, B. Jiao, X. Hou, J. Li, Z. Wu, *ACS Energy Lett.* **2020**, *5*, 1062.

[41] J. Park, H. Ham, C. Park, *Org. Electron.* **2011**, *12*, 227.

[42] J. Ràfols-Ribé, P.-A. Will, C. Hänisch, M. Gonzalez-Silveira, S. Lenk, J. Rodríguez-Viejo, S. Reineke, *Sci. Adv.* **2018**, *4*, eaar8332.

[43] D. L. Rode, *Phys. Rev. B* **1970**, *2*, 4036.

[44] C. D. Lokhande, P. S. Patil, H. Tributsch, *Appl. Surf. Sci.* **1998**, *123–124*, 294.

[45] R. Chen, J. Cao, Y. Duan, Y. Hui, T. T. Chuong, D. Ou, F. Han, F. Cheng, X. Huang, B. Wu, N. Zheng, *J. Am. Chem. Soc.* **2019**, *141*, 541.

[46] X. Li, J. Yang, Q. Jiang, H. Lai, S. Li, J. Xin, W. Chu, J. Hou, *ACS Nano* **2018**, *12*, 5605.

[47] M. Aven, *J. Appl. Phys.* **1971**, *42*, 1204.

[48] Z. Ning, H. Tian, C. Yuan, Y. Fu, H. Qin, L. Sun, H. Ågren, *Chem. Commun.* **2011**, *47*, 1536.

[49] X. Y. Chin, A. Perumal, A. Bruno, N. Yantara, S. A. Veldhuis, L. Martínez-Sarti, B. Chandran, V. Chirvony, A. S.-Z. Lo, J. So, C. Soci, M. Grätzel, H. J. Bolink, N. Mathews, S. G. Mhaisalkar, *Energy Environ. Sci.* **2018**, *11*, 1770.

[50] F. Yan, J. Xing, G. Xing, L. Quan, S. T. Tan, J. Zhao, R. Su, L. Zhang, S. Chen, Y. Zhao, A. Huan, E. H. Sargent, Q. Xiong, H. V. Demir, *Nano Lett.* **2018**, *18*, 3157.

[51] Z. Wei, A. Perumal, R. Su, S. Sushant, J. Xing, Q. Zhang, S. T. Tan, H. V. Demir, Q. Xiong, *Nanoscale* **2016**, *8*, 18021.

[52] X. Zhang, W. Wang, B. Xu, S. Liu, H. Dai, D. Bian, S. Chen, K. Wang, X. W. Sun, *Nano Energy* **2017**, *37*, 40.

[53] S. Lee, J. H. Park, Y. S. Nam, B. R. Lee, B. Zhao, D. D. Nuzzo, E. D. Jung, H. Jeon, J.-Y. Kim, H. Y. Jeong, R. H. Friend, M. H. Song, *ACS Nano* **2018**, *12*, 3417.

[54] H. Cho, C. Wolf, J. S. Kim, H. J. Yun, J. S. Bae, H. Kim, J.-M. Heo, S. Ahn, T.-W. Lee, *Adv. Mater.* **2017**, *29*, 1700579.

[55] Y.-Y. Zhang, S. Chen, P. Xu, H. Xiang, X.-G. Gong, A. Walsh, S.-H. Wei, *Chin. Phys. Lett.* **2018**, *35*, 036104.

[56] M. Kulbak, S. Gupta, N. Kedem, I. Levine, T. Bendikov, G. Hodes, D. Cahen, *J. Phys. Chem. Lett.* **2016**, *7*, 167.

[57] Y. Hu, E. M. Hutter, P. Rieder, I. Grill, J. Hanisch, M. F. Aygüler, A. G. Hufnagel, M. Handloser, T. Bein, A. Hartschuh, K. Tvingstedt, V. Dyakonov, A. Baumann, T. J. Savenije, M. L. Petrus, P. Docampo, *Adv. Energy Mater.* **2018**, *8*, 1870073.

[58] W. Li, M. U. Rothmann, A. Liu, Z. Wang, Y. Zhang, A. R. Pascoe, J. Lu, L. Jiang, Y. Chen, F. Huang, Y. Peng, Q. Bao, J. Etheridge, U. Bach, Y.-B. Cheng, *Adv. Energy Mater.* **2017**, *7*, 1700946.

[59] M. B. Huang, K. McDonald, J. C. Keay, Y. Q. Wang, S. J. Rosenthal, R. A. Weller, L. C. Feldman, *Appl. Phys. Lett.* **1998**, *73*, 2914.

[60] S. T. Lee, Z. Q. Gao, L. S. Hung, *Appl. Phys. Lett.* **1999**, *75*, 1404.

[61] S.-J. Chua, L. Ke, R. S. Kumar, K. Zhang, *Appl. Phys. Lett.* **2002**, *81*, 1119.